Scilight

Smart Materials and Devices

https://www.sciltp.com/journals/smd

Article

The Annealing Influence on the Mechanical Behavior of $Ni_{45}Co_{23}Cr_{20}Mo_5Al_7$ Medium-Entropy Alloy

Meiling Liang [1,2], Hongmin Zhang [1,2], Peter K. Liaw [3], Fanchao Meng [1,2,*] and Shuying Chen [1,2,*]

[1] Institute for Advanced Studies in Precision Materials, Yantai University, Yantai 264005, China
[2] Shandong Key Laboratory of Advanced Structural Materials Genome Engineering, Yantai University, Yantai 264005, China
[3] Department of Materials Science and Engineering, The University of Tennessee, Knoxville, TN 37996, USA
* Correspondence: mengfanchao@ytu.edu.cn (F.M.); sychen@ytu.edu.cn (S.C.)

How To Cite: Liang, M.; Zhang, H.; Liaw, P.K.; et al. The Annealing Influence on the Mechanical Behavior of $Ni_{45}Co_{23}Cr_{20}Mo_5Al_7$ Medium-Entropy Alloy. *Smart Materials and Devices* **2026**, *1*(1), 5.

Received: 24 December 2025
Revised: 16 February 2026
Accepted: 27 February 2026
Published: 20 March 2026

Abstract: The influence of heat treatment on the mechanical properties of a novel $Ni_{45}Co_{23}Cr_{20}Mo_5Al_7$ medium-entropy alloy (MEA) has been systematically investigated. An exceptional combination of ultimate tensile strength (UTS) of approximately 1.3 GPa and ductility of approximately 13% was achieved through annealing at 850 °C for 2 h followed by aging at 780 °C for 8 h, which produces a partially recrystallized microstructure with uniformly distributed precipitates. The superior mechanical performance results from the synergistic contribution of retained deformation twins and stacking faults from cold rolling, precipitation hardening, and fine recrystallized grains. In the non-recrystallized condition annealed at 800 °C for 4 h, an extremely high UTS of approximately 1.55 GPa was obtained, attributed to the preferential segregation of Mo to deformation twins and stacking faults, which substantially increases the resistance to dislocation motion. However, this condition exhibited negligible ductility. The fully recrystallized condition achieved through annealing at 900 °C followed by aging at 780 °C resulted in a balanced combination of UTS of approximately 1.2 GPa and ductility of approximately 28%, governed by precipitation hardening and recrystallized grain size. This study demonstrates a viable heat treatment strategy for developing high-performance MEAs that overcome the conventional strength-ductility trade-off.

Keywords: medium-entropy alloy; tensile properties; precipitate hardening

1. Introduction

The high-entropy alloys (HEAs) with single-phase solid solution were proposed by Yeh et al. in 2004, which consist of multiple principal elements in an equimolar or near-equimolar ratio [1]. It is comprehensively investigated that HEAs possess excellent mechanical properties [2–4], attractive phase stability at elevated temperatures, and outstanding resistance to corrosion, oxidation, and irradiation [5–8]. The most studied Cantor alloy of CoCrFeNiMn draw much attention to twin-induced plasticity (TWIP), transformation-induced plasticity (TRIP), precipitation hardening, and heterostructure hardening [9]. The subset of Cantor alloy, CoCrNi medium entropy alloy (MEA), presents superior mechanical behavior at both room and cryogenic temperature compared with Cantor alloy, which was due to the lower stacking fault energy and earlier occurrence of nano-twinning during the deformation process [10,11].

Despite these promising characteristics, a critical challenge remains in developing CoCrNi-based alloys that simultaneously achieve high strength and substantial ductility at room temperature. While the baseline CoCrNi MEA exhibits excellent ductility, its room-temperature strength is often insufficient for advanced engineering applications. Conversely, strategies to enhance strength through severe plastic deformation frequently result in substantial ductility loss, limiting their practical utility. This strength-ductility trade-off represents a persistent

obstacle in materials design that requires innovative approaches combining multiple strengthening mechanisms in a synergistic manner.

To address this challenge, researchers have increasingly dedicated their efforts to designing new alloys based on the CoCrNi MEA through strategic compositional modifications. The minor addition of elements such as Ti, Al, C, or B has been frequently employed to tune the stacking fault energy as well as control precipitate evolution [12–15], demonstrating that alloying elements can significantly improve mechanical properties. Another effective strategy to increase tensile strength involves the incorporation of large-radius elements to produce severe atomic size mismatch as well as modulus mismatch effects. Ming et al. investigated the heat treatment effect on the mechanical properties in $Cr_{15}Fe_{20}Co_{35}Ni_{20}Mo_{10}$ alloys. The enhanced tensile strength of 1.4 GPa and ductility of ~12% were attributed to the coupling solid solution hardening, nano-twinning, and precipitation hardening mechanisms [16]. Similarly, Liu et al. studied the CoCrFeNi alloy with the addition of Mo element and obtained a good combination of tensile strength of ~1.2 GPa and ductility of ~19%. Such surprising mechanical properties were due to the hard intermetallic particles as well as the heavily distorted lattice in the matrix [17].

Building upon these developments, the present study introduces a novel $Ni_{45}Co_{23}Cr_{20}Mo_5Al_7$ MEA designed to synergistically integrate multiple strengthening mechanisms. The novelty of this alloy lies in its carefully tailored composition that distinguishes it from conventional equimolar CoCrNi systems. The enrichment of Ni content to 45 at.% establishes it as the primary matrix element, while the incorporation of 5 at.% Mo introduces severe atomic size mismatch effects and enables preferential segregation to crystallographic defects during aging treatment. Meanwhile, the addition of 7 at.% Al facilitates the formation of coherent $L1_2$ precipitates for effective precipitation hardening. This particular combination has not been previously explored and represents a systematic approach to overcoming the strength-ductility trade-off.

The primary motivation for this work stems from the need to establish how controlled microstructural heterogeneity can achieve exceptional mechanical performance. While previous studies have investigated either precipitation hardening or recrystallization behavior independently, there remains a significant gap in understanding how to systematically combine partial recrystallization with optimized precipitation. Therefore, the present study aims to reveal the influence of various heat treatment strategies on the mechanical behavior of the $Ni_{45}Co_{23}Cr_{20}Mo_5Al_7$ alloy. Through systematic characterization using EBSD and mechanical property evaluation, we seek to establish the structure-property relationships that govern the simultaneous achievement of high strength and substantial ductility, thereby providing practical guidance for designing high-performance MEAs for advanced structural applications.

2. Experimental Procedure

The $Ni_{45}Co_{23}Cr_{20}Mo_5Al_7$ (at.%) alloy was prepared by the arc-melting technique under a highly pure argon atmosphere. The purity for each element is at least 99.95%, and the ingot was re-melted five times to guarantee chemical homogeneity. Then, the as-cast ingots were undergone homogenization treatment at 1200 °C for 24 h followed by water quenching (WQ). Subsequently, the homogenized samples were cold-rolled into a thin sheet with a total thickness reduction of 81%. Finally, the cold-rolled sheets were rapidly heated to 800 °C for 4 h (CRA), 900 °C for 2 h to obtain recrystallized grains, and then aged at 650 and 780 °C for 8 h (CRRA), and 850 °C for 2 h to acquire partially recrystallized grain and then aged at 780 °C for 8 h (CRPRA). The microstructures of the $Ni_{45}Co_{23}Cr_{20}Mo_5Al_7$ alloy were characterized by scanning electron microscope (SEM, Tescan Amber, Brno, Czechia) and electron backscattered diffraction (EBSD, Oxford, Abingdon, UK) at an accelerating voltage of 20 kV, a working distance of 11 mm, and step sizes between 0.08 and 1 μm. The specimen was ground with the wet SiC abrasive paper of # 600, 800, and 1200. The specimens used for SEM and EBSD characterization were finally polished using progressively finer SiO_2 suspensions down to 0.05 μm. Grain size measurements were performed on SEM micrographs using the linear intercept method according to ASTM E112 standard. For each heat treatment condition, at least 5 different regions were analyzed to ensure statistical reliability. The average grain size and standard deviation were calculated from multiple measurements. Microhardness was measured using a Vickers microhardness tester with a load of 100 g and a dwell time of 5 s. Additionally, the spacing between adjacent indentations was maintained at a minimum of 500 μm (five times the indentation diagonal length) to avoid interference from the plastic deformation zone of neighboring indentations. For each condition, at least ten measurements were performed at different locations. Flat dog-bone-shaped specimens with a gauge length of 20 mm, a width of 3.5, and 1.5 mm in thickness were fabricated by electron-discharge machining (EDM) from the sheets along the rolling direction (RD). Tensile tests, at room temperatures, were performed on a Sens tensile machine under a tensile strain rate of 1×10^{-3} s^{-1}.

3. Results and Discussion

To start with, the recrystallization temperature was determined by the microhardness at various annealing temperatures. As shown in Figure 1, a sudden drop of hardness happens at the annealing temperature of 900 °C, indicating that the recrystallization of the present alloy starts around 900 °C. It was reported that the recrystallization temperature in $CoCrNiAl_{0.1}Mo_{0.1}$ was in the temperature range 600–700 °C, which was lower than that of the present alloy. The recrystallization temperature in the present work was chosen as 900 °C for 2 h. Moreover, the microhardness was carried out again at various aging temperatures to estimate the optimum condition for precipitation hardening of the present alloy. Figure 1b showed the evolution of hardness as a function of aging temperature. It was evident that there was a hardness peak at 780 °C, and steadily decreases with increasing aging temperature to 850 °C, indicating that the aging treatment at 780 °C presented the highest microhardness with a remarkable precipitation-strengthening effect. Then, the alloy aged at 780 °C was subsequently chosen for the tensile experiment at room temperature. In order to enhance to hardening effect of $Ni_{45}Co_{23}Cr_{20}Mo_5Al_7$, the hetero-structure with partially recrystallized grains was obtained by annealing at 850 °C for 2 h and aging at 780 °C.

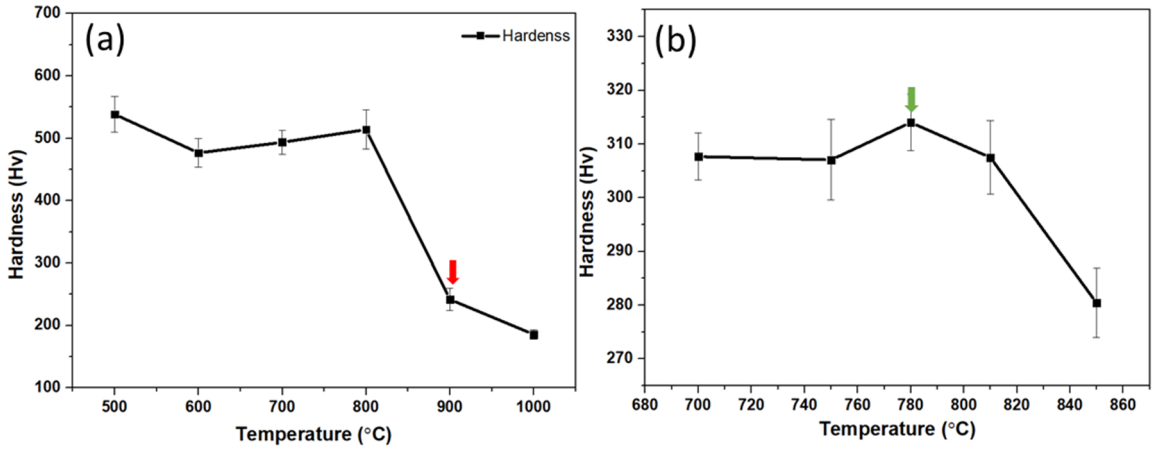

Figure 1. The hardness of cold-rolled $Ni_{45}Co_{23}Cr_{20}Mo_5Al_7$ alloy (**a**) annealed at various temperatures with the red arrow indicating the sudden drop of hardness at 900 °C. (**b**) Annealed at 900 °C and then aged at different temperatures for 2 h, with the green arrow representing the maximum hardness at 780 °C.

The microstructure before the tensile tests was displayed in Figure 2. The heavily deformed microstructure without recrystallized grains was found in CRA. Evident precipitates (shown in the inset), as well as multiple deformation twins (indicated by red arrow), were observed in Figure 2a. In the CRPRA alloy, partially recrystallized structures with deformed twins and very small grains were obtained, as shown in Figure 2b. Major $L1_2$ precipitates were generated in the recrystallized grains, as indicated by the red circle and in the inset [18]. It was previously studied that in the fully recrystallized matrix of $Al_{0.3}CoCrFeNi$ alloy, most $L1_2$ phases were formed and the formation of the $L1_2$ phase was favored due to a higher homogeneous nucleation rate compared to another competing equilibrium phase [19]. In the CRRA sample of annealed 900 °C and aged at 780 °C, full recrystallized grains were obtained with a grain size of ~14 μm. In the magnified image of the inset, a large number of precipitates were present at the grain boundaries and within the grain interior. Similar precipitates were confirmed as $L1_2$ in $CoCrNiAl_{0.1}Mo_{0.1}$ as well [18]. Annealing twins were frequently observed in the matrix. Figure 2d showed the microstructure of the specimen heat treated at 900 °C for 2 h and aged at 650 °C for 4 h. No apparent precipitates were found. However, it was reported that a large amount of $L1_2$ phase formed in $CoCrNiAl_{0.1}Mo_{0.1}$ when annealed at 600 °C for 24 h after 1100 °C—recrystallization. With the annealing time extending to 144 h, another precipitate of μ formed as well, which implied that $L1_2$ was dynamically unstable and tends to form compared with μ phase [18]. The absence of $L1_2$ in the present work might be due to the short annealing time and the negligible content in the matrix.

The representative tensile engineering stress-strain curves are shown in Figure 3. It is evident that the alloy of CRA alloy exhibits the highest tensile strength, with an UTS of ~1.55 GPa without any ductility. Such high strength and low ductility were due to the extremely high density of dislocation substructure from the cold rolling process. No recrystallization occurred to release the high-stress concentration. It was suggested that the heavily deformed Mo-containing alloy showed larger vacancy concentrations and deformation twins that assist short-range self-diffusion. When aged at 800 °C, the alloying element Mo was proposed to preferentially segregate at

deformation twins and stacking faults. The produced vacancies and short diffusion distances could explain the rapid diffusion of Mo during aging treatment. In addition, the segregation of Mo elements at twins and stacking faults significantly increased the barrier of mobile dislocation, which resulted in the improvement of strength and a reduction of ductility [20].

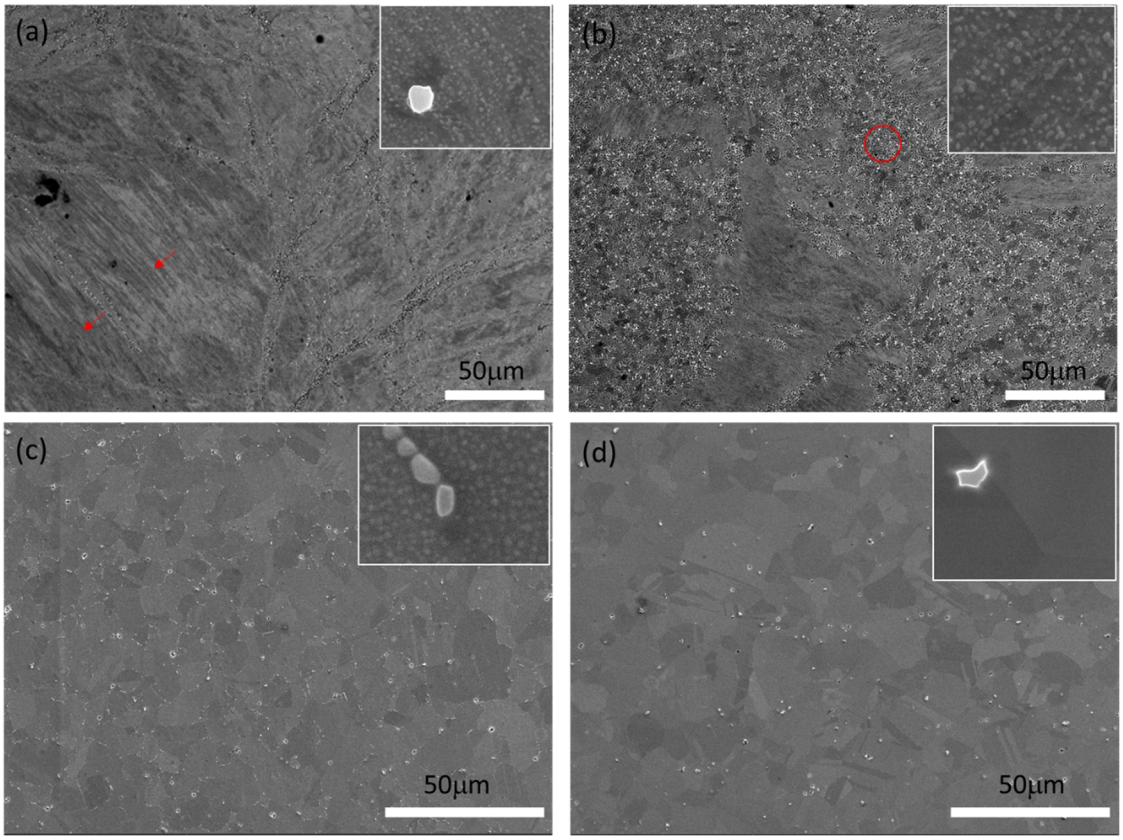

Figure 2. The microstructure before tensile tests. (**a**) annealed at 800 °C for 4 h, (**b**) annealed at 850 °C for 2 h and aged at 780 °C for 8 h, (**c**) annealed at 900 °C for 2 h and aged at 780 °C for 8 h, (**d**) annealed at 900 °C for 2 h and aged at 650 °C for 8 h.

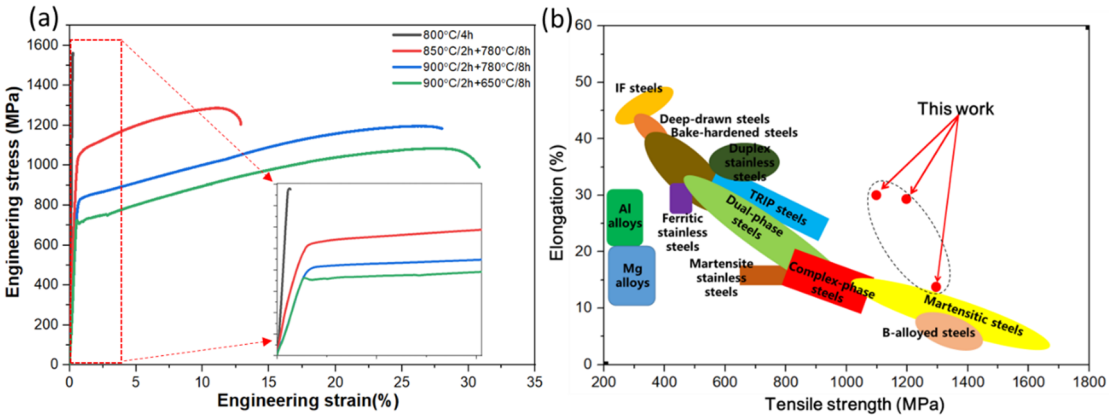

Figure 3. (**a**) The representative tensile stress-strain curve of $Ni_{45}Co_{23}Cr_{20}Mo_5Al_7$ under various conditions, (**b**) Comparison of mechanical properties with other advanced steels.

The specimen annealed at 850 °C and aged at 780 °C displayed the best synergetic strength and ductility, with a ~1.3GPa in UTS, yield stress (YS) of 1.05 GPa, and ductility of ~13%. The enhanced ductility was attributed to the partially recrystallized grains, as indicated in Figure 2c. The remaining deformation twins, stacking faults, and high density of dislocation would contribute to the high yield stress. The occurrence of precipitates in the recrystallized grains favored the precipitate hardening during the tensile loading. The specimen annealed at 900 °C for 2 h and aging at 780 °C and 650 °C for 8 h, respectively, presented a similar tensile behavior, except for the different UTS and yield stress. The alloy aging at 780 °C showed higher tensile stress of ~1.2 GPa without loss in

ductility, compared with that aging at 650 °C. Both alloys before tensile tests exhibit the recrystallized microstructure with a grain size of ~15–20 μm. The distinct difference between them was the appearance of precipitates in the matrix. It is evident that alloy aged at 780 °C shows uniformly distributed $L1_2$ particles at the grain boundaries and within the grain interior, which will significantly enhance the precipitate hardening, then the tensile strength. However, due to the full recrystallization with low density of dislocation substructure, twins, and stacking faults in both alloys, the yield strength in CRRA was lower than that of CRPRA alloy. The direct comparison of UTS and elongation in $Ni_{45}Co_{23}Cr_{20}Mo_5Al_7$ alloy and other reported advanced steels is illustrated in the strength-ductility diagram in Figure 3b. The wide range of mechanical properties in $Ni_{45}Co_{23}Cr_{20}Mo_5Al_7$ alloy was achieved by designing three processing conditions. It is evident that the present alloy is located at the upper-right above the previously studied alloys, clearly indicating that they are superior to most conventional advanced steels.

The typical EBSD images of deformed specimens under various conditions were presented in the Figure 4. Intensive deformation twins indicated by the white arrow in the Figure 4a remained in the sample aged at 800 °C for 4 h, without any recrystallized grains, resulting in extremely high yield stress but low ductility, as observed in Figure 3. In the specimen annealed at 850 °C and aged at 780 °C partially recrystallized microstructure was found, as indicated by the white and black arrow in Figure 4d,e. The recrystallized grain is significantly small, about 2–3 μm, with the released stress concentration, as indicated by a black arrow in Figure 4e. The kernel average misorientation (KAM) in the EBSD measurement represented the density of geometrically necessary dislocations. In the region of un-recrystallization, the high density of KAM implied the heavily distorted grains with multiple defects, including a high density of dislocations, deformation twins, and stacking fault, resulting in more obstacles to the dislocation movement. Figure 4g presented the deformed structure in the fully recrystallized specimen of annealed at 900 °C for 2 h, with a grain size of ~8 μm. No deformation twins were found after being tested at room temperature. It was concluded that partial recrystallization by tuning the post-processing is an effective way to increase strength. However, it is essential to systematically investigate the precipitation hardening and partial recrystallization to achieve the best combination with excellent strength without reducing the ductility.

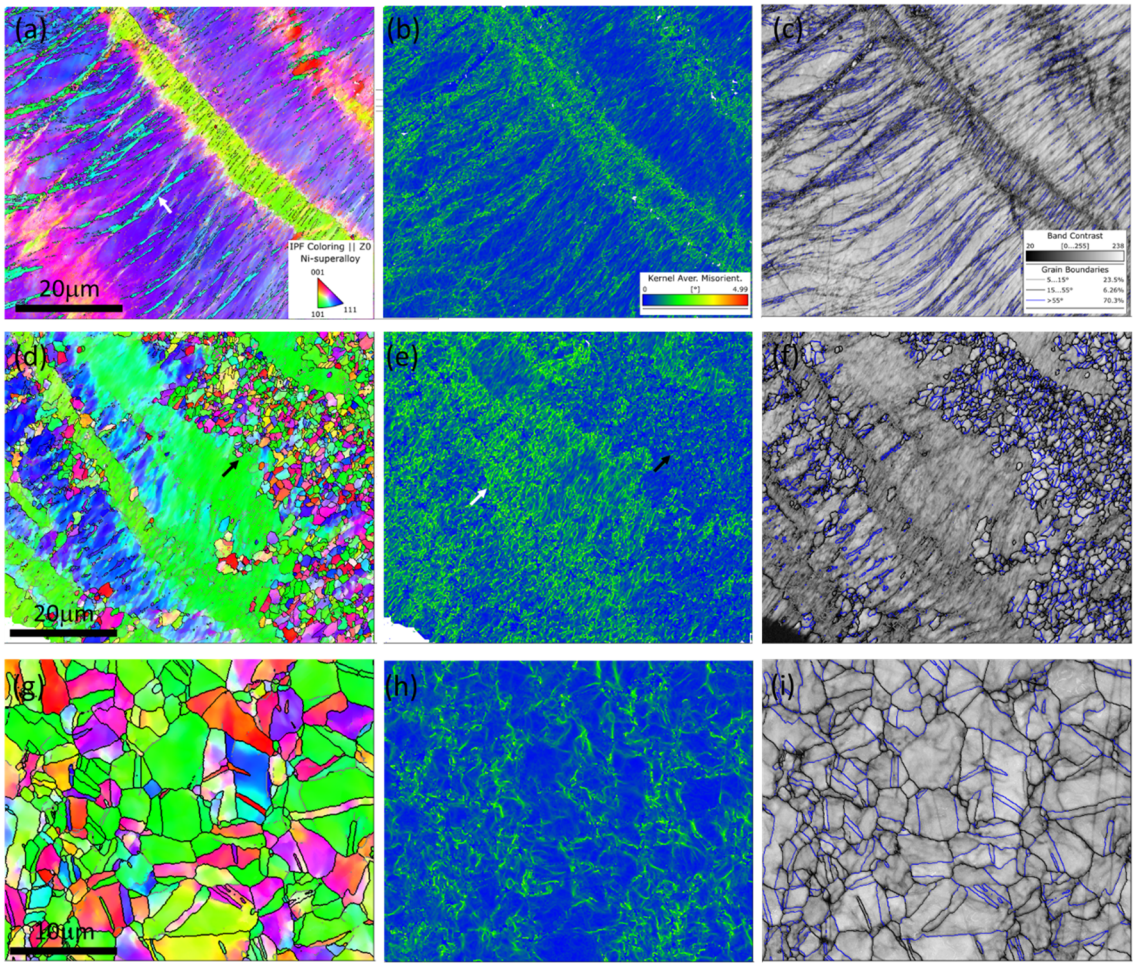

Figure 4. The EBSD image of the deformed specimen at room temperature. (**a**–**c**) aged at 800 °C for 4 h, (**d**–**f**) annealed at 850 °C for 2 h and aged at 780 °C for 8 h, (**g**–**i**) annealed at 900 °C for 2 h and aged at 780 °C for 8 h.

The microhardness measurements in Figure 1 effectively track microstructural changes during heat treatment. The sudden hardness drops at 900 °C (Figure 1a) corresponds to recrystallization onset. In the CRA condition (800 °C/4h), the hardness remains high because this temperature is below the recrystallization point. EBSD analysis (Figure 4a-c) confirms intensive deformation twins and high KAM values throughout the microstructure, indicating high dislocation density inherited from cold rolling. These features explain both the elevated hardness and the extremely high ultimate tensile strength of ~1.55 GPa (Figure 3a), but also the lack of ductility due to severely restricted dislocation mobility.

The aging treatment effect (Figure 1b) shows a hardness peak at 780 °C, correlating with optimal $L1_2$ precipitation. SEM observations (Figure 2) confirm uniformly distributed precipitates at 780 °C, while the 650 °C-aged sample shows no apparent precipitates despite full recrystallization. This difference directly translates to mechanical properties: the 780 °C-aged alloy exhibits higher strength (~1.2 GPa) compared to 650 °C aging, while both maintain ~28% ductility due to their fully recrystallized microstructures with low dislocation density (Figure 4g–i).

The optimal strength-ductility combination in CRPRA (UTS ~1.3 GPa, ductility ~13%) results from its heterogeneous microstructure. EBSD images (Figure 4d–f) reveal coexisting non-recrystallized regions with high KAM values and small recrystallized grains with low KAM values. The non-recrystallized regions with deformation twins, high dislocation density, and Mo segregation contribute to high yield stress (1.05 GPa), while the recrystallized regions with $L1_2$ precipitates and fine grain size provide additional strengthening. Critically, these recrystallized zones with low dislocation density accommodate plastic deformation and delay crack initiation, enabling superior ductility compared to CRA. This heterogeneous deformation behavior produces sustained strain hardening throughout the uniform elongation regime. The KAM maps provide quantitative correlation with mechanical response. In CRA (Figure 4c), uniformly high KAM values across the entire microstructure correspond to extremely high strength but zero ductility—the absence of low-KAM regions eliminates zones for plastic accommodation. The CRPRA condition (Figure 4f) exhibits heterogeneous KAM distribution, where high-KAM regions maintain yield strength while low-KAM regions enable ductility through strain partitioning during tensile deformation. The fully recrystallized CRRA condition (Figure 4i) shows uniform low KAM distribution, corresponding to moderate yield strength but excellent ductility (~28%).

In summary, the integrated analysis demonstrates that mechanical properties can be precisely tailored through controlled heat treatment. The partially recrystallized CRPRA microstructure represents an optimal strategy for overcoming the strength-ductility trade-off by synergistically combining retained dislocation substructures, precipitation hardening, grain refinement, and Mo segregation. The EBSD-measured KAM distributions provide direct evidence for heterogeneous strain distribution that enables this synergy, while hardness measurements serve as an effective tool for optimizing heat treatment parameters.

4. Conclusions

This study systematically investigated the mechanical properties of a novel $Ni_{45}Co_{23}Cr_{20}Mo_5Al_7$ MEA subjected to various heat treatment conditions. The partially recrystallized condition exhibited an exceptional combination of UTS of approximately 1.3 GPa and ductility of approximately 13%, originating from the synergistic contribution of retained deformation twins, uniformly distributed precipitates, and fine recrystallized grains. The coexistence of high-dislocation-density non-recrystallized zones and low-dislocation-density recrystallized zones enables effective strain partitioning, thereby overcoming the conventional strength-ductility trade-off. The non-recrystallized condition demonstrated an extraordinarily high UTS of approximately 1.55 GPa due to preferential Mo segregation to deformation twins and stacking faults, but exhibited negligible ductility. The fully recrystallized condition yielded a balanced combination of UTS of approximately 1.2 GPa and ductility of approximately 28%, governed by precipitation hardening and grain refinement. This work demonstrates that tailored heat treatment strategies can effectively design heterogeneous microstructures that synergistically integrate multiple strengthening mechanisms for high-performance medium-entropy alloys.

Author Contributions

M.L.: data curation, investigation, writing—original draft preparation; H.Z.: data curation, methodology, investigation; P.K.L.: writing-review & editing; F.M.: supervision, writing—reviewing and editing; S.C.: funding acquisition, supervision, writing—original draft preparation. All authors have read and agreed to the published version of the manuscript.

Funding

This research was funded by National Natural Science Foundation of China (Grant No. 52371163), Taishan ScFholars Program of Shandong Province (tsqn202408154), and Yantai city matching fund for Taishan Scholars Program of Shandong Province, China.

Data Availability Statement

Data contained in this paper are available upon request to the corresponding author.

Conflicts of Interest

Given the role as the Editorial Board member, Shuying Chen had no involvement in the peer review of this paper and had no access to information regarding its peer-review process. Full responsibility for the editorial process of this paper was delegated to another editor of the journal.

Use of AI and AI-Assisted Technologies

No AI tools were utilized for this paper.

References

1. Yeh, J.-W.; Chen, S.-K.; Lin, S.-J.; et al. Nanostructured High-Entropy Alloys with Multiple Principal Elements: Novel Alloy Design Concepts and Outcomes. *Adv. Eng. Mater.* **2004**, *6*, 299–303. https://doi.org/10.1002/adem.200300567.
2. Otto, F.; Dlouhý, A.; Somsen, C.; et al. The influences of temperature and microstructure on the tensile properties of a CoCrFeMnNi high-entropy alloy. *Acta Mater.* **2013**, *61*, 5743–5755. https://doi.org/10.1016/j.actamat.2013.06.018.
3. Gludovatz, B.; Hohenwarter, A.; Catoor, D.; et al. A fracture-resistant high-entropy alloy for cryogenic applications. *Science* **2014**, *345*, 1153–1158. https://doi.org/10.1126/science.1254581.
4. Li, Z.; Pradeep, K.G.; Deng, Y.; et al. Metastable high-entropy dual-phase alloys overcome the strength-ductility trade-off. *Nature* **2016**, *534*, 227–230. https://doi.org/10.1038/nature17981.
5. Pandey, P.; Kashyap, S.; Palanisamy, D.; et al. On the high temperature coarsening kinetics of γ′ precipitates in a high strength $Co_{37.6}Ni_{35.4}Al_{9.9}Mo_{4.9}Cr_{5.9}Ta_{2.8}Ti_{3.5}$ fcc-based high entropy alloy. *Acta Mater.* **2019**, *177*, 82–95. https://doi.org/10.1016/j.actamat.2019.07.011.
6. Fu, A.; Liu, B.; Lu, W.; et al. A novel supersaturated medium entropy alloy with superior tensile properties and corrosion resistance. *Scr. Mater.* **2020**, *186*, 381–386. https://doi.org/10.1016/j.scriptamat.2020.05.022.
7. Kai, W.; Li, C.C.; Cheng, F.P.; et al. Air-oxidation of FeCoNiCr-based quinary high-entropy alloys at 700–900 °C. *Corros. Sci.* **2017**, *121*, 116–125. https://doi.org/10.1016/j.corsci.2017.02.008.
8. Lin, Y.; Yang, T.; Lang, L.; et al. Enhanced radiation tolerance of the Ni-Co-Cr-Fe high-entropy alloy as revealed from primary damage. *Acta Mater.* **2020**, *196*, 133–143. https://doi.org/10.1016/j.actamat.2020.06.027.
9. Cantor, B. Multicomponent high-entropy Cantor alloys. *Prog. Mater. Sci.* **2020**, *120*, 100754. https://doi.org/10.1016/j.pmatsci.2020.100754.
10. Yoshida, S.; Bhattacharjee, T.; Bai, Y.; et al. Friction stress and Hall-Petch relationship in CoCrNi equi-atomic medium entropy alloy processed by severe plastic deformation and subsequent annealing. *Scr. Mater.* **2017**, *134*, 33–36. https://doi.org/10.1016/j.scriptamat.2017.02.037.
11. Laplanche, G.; Kostka, A.; Reinhart, C.; et al. Reasons for the superior mechanical properties of medium-entropy CrCoNi compared to high-entropy CrMnFeCoNi. *Acta Mater.* **2017**, *128*, 292–303. https://doi.org/10.1016/j.actamat.2017.02.036.
12. Sun, Y.; Wang, C.; Shi, C.; et al. Effects of Ti on the ageing microstructure and mechanical properties of Ni-Co-Cr-Ti multi-principal element alloy. *Mater. Sci. Eng. A* **2025**, *927*, 148007. https://doi.org/10.1016/j.msea.2025.148007.
13. Li, Y.; Liang, M.; Tong, Y.; et al. Cost-effective design of high-performance NiCoCrAlTi high-entropy alloys through Fe-mediated phase competition control: A combined experimental and first-principles study. *Mater. Futures* **2026**, *5*, 015004. https://doi.org/10.1088/2752-5724/ae2a58.
14. Zhang, H.; Meng, H.; Meng, F.; et al. Magnificent tensile strength and ductility synergy in a NiCoCrAlTi high-entropy alloy at elevated temperature. *J. Mater. Res. Technol.* **2024**, *28*, 522–532. https://doi.org/10.1016/j.jmrt.2023.12.001.
15. Wu, X.; Sun, Z.; Guo, W.; et al. Microstructural origin of the simultaneous enhancements in strength and ductility of a nitrogen-doped high-entropy alloy. *Acta Mater.* **2026**, *304*, 121753. https://doi.org/10.1016/j.actamat.2025.121753.
16. Ming, K.; Bi, X.; Wang, J. Precipitation strengthening of ductile $Cr_{15}Fe_{20}Co_{35}Ni_{20}Mo_{10}$ alloys. *Scr. Mater.* **2017**, *137*, 88–93. https://doi.org/10.1016/j.scriptamat.2017.04.035.
17. Liu, W.H.; Lu, Z.P.; He, J.Y.; et al. Ductile $CoCrFeNiMo_x$ high entropy alloys strengthened by hard intermetallic phases. *Acta Mater.* **2016**, *116*, 332–342. https://doi.org/10.1016/j.actamat.2016.06.063.

18. Liu, X.S.; Li, R.; Lu, Y.; et al. Spinodal decomposition induced nanoprecipitates strengthened CoCrNi-base medium entropy alloy. *Mater. Sci. Eng. A* **2021**, *822*, 141674. https://doi.org/10.1016/j.msea.2021.141674.
19. Gwalani, B.; Gorsse, S.; Choudhuri, D.; et al. Modifying transformation pathways in high entropy alloys or complex concentrated alloys via thermo-mechanical processing. *Acta Mater.* **2018**, *153*, 169–185. https://doi.org/10.1016/j.actamat.2018.04.051.
20. Sorensen, D.; Li, B.Q.; Gerberich, W.W.; et al. Investigation of secondary hardening in Co–35Ni–20Cr–10Mo alloy using analytical scanning transmission electron microscopy. *Acta Mater.* **2014**, *63*, 63–72. https://doi.org/10.1016/j.actamat.2013.09.043.